PAPER

Quantum interference of electrons through electric-field-induced edge states in stacked graphene nanoribbons

To cite this article: Mai-Chung Nguyen and Huy-Viet Nguyen 2022 *Phys. Scr.* **97** 115814

Physica Scripta

PAPER

Quantum interference of electrons through electric-field-induced edge states in stacked graphene nanoribbons

RECEIVED
12 August 2022

REVISED
20 September 2022

ACCEPTED FOR PUBLICATION
11 October 2022

PUBLISHED
20 October 2022

Mai-Chung Nguyen[1,2,*] **and Huy-Viet Nguyen**[3,*]

[1] Graduate University of Science and Technology, Vietnam Academy of Science and Technology, Hoang Quoc Viet, Cau Giay, Hanoi, Vietnam
[2] Energy Department, University of Science and Technology of Hanoi, Vietnam Academy of Science and Technology, Hoang Quoc Viet, Cau Giay, Hanoi, Vietnam
[3] Institute of Physics, Vietnam Academy of Science and Technology, Hoang Quoc Viet, Cau Giay, Hanoi, Vietnam
[*] Authors to whom any correspondence should be addressed.

E-mail: nguyen-mai.chung@usth.edu.vn **and** nhviet@iop.vast.vn

Keywords: graphene, edge states, quantum interference, interferometers, Green's functions, tight-binding model

Abstract

In this work, we investigate, by means of numerical simulations, the quantum interference of electrons in stacked graphene structures consisting of two unequal width, armchair-edged graphene nanoribbons. Electronic states residing near the edges of the system are induced when an external electric field is applied normal to the ribbons. By reversing the direction of electric field in the central region, one can create an electronic analogue of the optical Fabry-Pérot (FP) interferometer. Electronic junctions formed at the boundaries between the central region and the left and right ones in the former play the role of the partially reflected mirrors in the latter. The observed conductance oscillations demonstrate that electrons in the edge states transporting through the system experience quantum interference similar to that of light waves passing through an optical FP interferometer. Moreover, electronic states formed at the junctions enhance inter-edge scattering which affects electron transmission significantly. The possibility to control electron transport via electric gates is also considered.

1. Introduction

Quantum interference is a manifestation of the wave nature of particles. In condensed-matter physics, quantum interference of electrons has been convincingly demonstrated in many systems, notably in the context of the Aharonov–Bohm (AB) effect [1, 2]. In order to observe electron interference, experiments should be performed in systems with large electron coherent lengths. In this regard, quantum Hall (QH) devices are of particular interest due to their ideal one-dimensional chiral edge states of two-dimensional (2D) electron systems, typically formed in complex semiconductor heterostructures when a strong perpendicular magnetic field is applied [3]. The successful isolation of graphene by Geim and Novoselov almost two decades ago [4] has opened a new world, thanks to its unique electronic properties [5], for demonstrations and studies of quantum interference of electrons [6]. With the special conical shape, i.e. linear energy dispersion, of conduction and valence bands that touch at six points in the Brillouin zone [5], low-energy electrons in graphene behave like massless relativistic Dirac fermions. As a consequence, 2D electron system in graphene when subjected to a strong magnetic field shows unconventional quantised Hall conductivity with half-integer filling factors [7, 8], compared to the integer ones for the case of conventional 2D electron system in semiconductor interfaces [3]. Remarkably, AB interferometers based on various graphene structures such as *p-n* junctions [9–12], magnetic junctions in stepped graphene [13] or polycrystalline graphene [14] have been proposed and demonstrated to work in the quantum Hall regime. In these setups, a mechanism for electron transmission between two edges has been introduced and, depending on the phase that electrons acquired when traversing in a magnetic field, they can interfere either constructively or destructively, leading to oscillations in electronic conductance or resistance. It

is worth to note that inter-edge scattering of quantum Hall edge states at the *p-n* junctions in the bipolar regime can lead to interesting phenomena such as fractional QH conductance plateaus at high magnetic fields [15].

Being a truly 2D material with semimetal character is also advantageous in that charge carrier density in graphene can be varied continuously by changing external (local) gate voltages, which allows for creating and controlling graphene *p-n* junctions in both unipolar and bipolar regimes. Furthermore, large electron mean-free path—of the order of ten microns when encapsulated in hexagonal boron nitride [16]—makes graphene an ideal platform for the experimental observation of ballistic electron interferences that has been proven difficult to achieve in other 2D electron systems. In ballistic interferences, electrons travel without being scattered, thus no phase changes, unless reflected at a barrier. A typical setup for achieving this type of interference is the electronic Fabry-Pérot (FP) interferometer in which graphene *p-n* junctions play the role of partially reflected mirrors in the optical counterpart for interference of light waves [17]. Electrons bouncing back and forth in the cavity can interfere, resulting in oscillations in electronic conductance or resistance. Experimental observations have been carried out in setups using both usual gate-induced [6, 18, 19] and tip-induced circular *p-n* junctions [20, 21]. Indeed, FP interference patterns have been employed as a means to detect relativistic quantum effects such as Klein tunneling [6, 19, 22].

Besides monolayer graphene, bilayer graphene has also been subject of extensive study. One of the attractive properties of graphene bilayer is the possibility to open and control the electronic bandgap using an external perpendicular electric field [23]. Moreover, it has been proposed that the domain wall between two oppositely biased bilayer graphene can host one-dimensional (1D) topological states [24] and this structure has been proven to be equivalent to the domain wall between AB- and BA-stacked bilayer graphene under a uniform electric field [25]. This 1D conducting channel can be exploited to make electron transmission between spatially-separated edge states in electronic FP interferometers. From an experimental standpoint, it would be desirable if edge states can be created without using a strong external magnetic field as in the case of QH FP interferometers. Thus we propose in this work a new electronic FP interferometer based on graphene bilayer structures consisting of two vertically stacked, unequal width armchair-edged graphene nanoribbons (GNR). We only consider AB-stacking structures as it has been proven to be energetically more favorable and focus on symmetrically-stacked configurations, i.e. those with a plane of reflection symmetry along the armchair direction, thus denoted as SS-AGNR. We shows that electronic states residing near the edges of SS-AGNR will be formed when a uniform electric field is applied perpendicularly to the structure. Transport properties of electron in these states through electronic FP interferometers created by applying perpendicular electric fields in opposite directions in different local regions are investigated using the Green's function technique within the Landauer's formalism. The oscillations observed in the conductance indicates quantum interference of electrons. Further analyses show that the interference is similar to that of light waves in an optical Fabry–Perot interferometer (FPI), but the interference is also affected significantly by the 1D conducting channels at the domain walls between two oppositely biased bilayer graphene. The rest of the paper is organized as follows: In section 2 we describe a tight-binding Hamiltonian for the system under study and briefly summarize necessary formulae for computing transport quantities like conductance, local density of states (LDoS) when employing the Green's function technique and the Landauer formalism to solve the Hamiltonian. In section 3, we present numerical results together with detailed analyses that help reveal the nature of quantum interference of electrons in this system. Finally, our conclusions are given in section 4.

2. Model and calculations

The structure of hetero-junctions studied in this work consists of there regions as schematically shown in figure 1. Electric fields are applied normal to all three regions, but the direction in the central region is opposite to those in the left and right ones. The width of the structure is determined by the number of carbon dimers of the top, M_t, and bottom, M_b, layers ($M_t < M_b$). The lengths of left, right, and central regions are determined by the number of unit cells and denoted by N_l, N_r, and N_c, respectively.

We adopt a tight-binding model to describe electrons in p_z-orbitals. Only nearest neighbor interactions are considered so as to keep the calculations simple without loss of physics involved. Under an external perpendicular electric field, the Hamiltonian reads

$$H_{tb} = t_{\parallel}\sum_{\langle i,j\rangle} c_i^{\dagger}c_j + t_{\perp}\sum_{\langle p,q\rangle} c_p^{\dagger}c_q + \frac{U}{2}\sum_{n,m}(c_n^{\dagger}c_n - c_m^{\dagger}c_m). \quad (1)$$

Here the first two terms represent in-plane and out-of-plane hopping energy wherein $\langle i,j\rangle$ and $\langle p,q\rangle$ denote nearest neighboring atoms in the same layer and in different layers, respectively. The values of intra-layer, $t_{\parallel}$, and inter-layer, $t_{\perp}$, hopping parameters are -2.7 and 0.39 eV, respectively [26]. The last term is the onsite energy due to external electric field with two indices n and m running over all atoms in different layers which is chosen

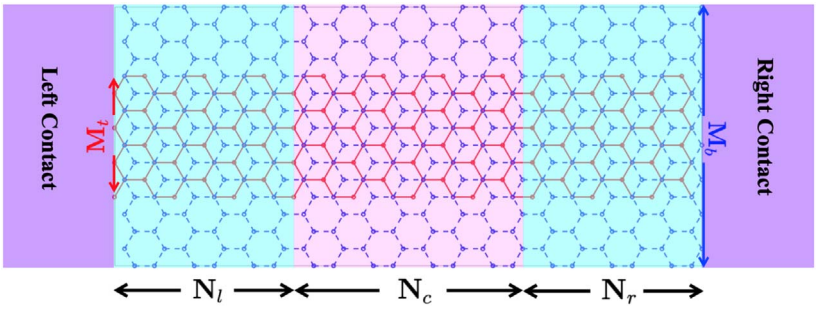

Figure 1. Schematic of electronic FP interferometers consisting of three regions with opposite local perpendicular electric fields which can be created using different local gates. The length of each region is determined by the number of unit cells (N_l, N_c and N_r for left, central and right regions, respectively.) The width of top and bottom layers are characterised by the number of carbon dimers M_t and M_b.

according to the direction of applied electric field. U is the electric potential difference between two layers with the zero being set at the middle and was varied in our study.

The Hamiltonian was solved by the Green's function technique [27, 28]. Since the calculations are performed for a finite structure, the Green's functions are not represented in momentum space; instead, the structure is divided into layers and the Green's functions for each layer are obtained recursively. In particular, the retarded Greens function is determined as

$$G^R(E) = [E + i0^+ - H_D - \Sigma_L - \Sigma_R]^{-1}. \tag{2}$$

Here H_D is the Hamiltonian of the device region and $\Sigma_{L,R}$ are self-energies describing the left and right device-to-lead couplings, respectively. The leads are assumed to be semi-infinite and the self-energies were computed employing the efficient iterative algorithm by Sancho-Rubio [29]. The local density of left (right) injected electronic states, $D_{L(R)}(E, r)$, are obtained as

$$D_{L(R)}(E, r) = \frac{G^R \Gamma_{L(R)} G^{R\dagger}}{2\pi}, \tag{3}$$

with $\Gamma_{L(R)} = i(\Gamma_{L(R)} - \Gamma^{\dagger}_{L(R)})$ being the injection rate of electrons at the left (right) contacts. The total LDoS can be computed by using either $D(E, r) = D_L(E, r) + D_R(E, r)$ or $D(E, r) = -\mathrm{Im}(G^R(E))/\pi$. Transport quantities like transmission probability, conductance were computed within the Landauer formalism as [27]

$$T(E) = \mathrm{Tr}[\Gamma_L G^R \Gamma_R G^{R\dagger}]. \tag{4}$$

3. Results and discussion

3.1. Band structures and edge states

We first investigate the effect of applied electric field on the electronic band structure of periodic SS-AGNRs as it will provide useful information for understanding the transport properties of electrons in the setup. Figure 2(a,b,c) shows electronic band structures of a SS-AGNR having the width of about 50 nm ($M_b = 200$ and $M_t = 174$) at different values of electric field. We note that the potential difference $U = 0.6$ V in figure 2(c) corresponds to a field strength of 1.8 V/nm which can be accessible in experiments [23, 30]. As clearly seen, the conduction and valence bands, touching at $k_x = 0$ in the absence of electric field in figure 2(a), are separated when finite electric field is applied in figures 2(b), (c). Moreover, there appear subbands in the gap region which suggests the formation of electronic states propagating near the edges of the ribbon only. This is confirmed by the pictures of LDoS in figure 2(d) where LDoS in the interior is much smaller than that near the edges. Since the subband do not connect the valence and conduction bands, these edge states are not topologically protected and can experience backscattering when incident to a potential barrier. This feature will be exploit to design an electronic analogue of optical FPI for electrons. We note in passing that the subband in the gap region is two-fold degenerate and this degeneracy will be lifted (not shown) in asymmetric stacked AGNRs. Furthermore, when the direction of applied electric field is reversed, the band structure will be reflected through the horizontal line at the energy $E = 0$. This feature will be useful to understand the quantum interference of electrons presented in the next subsection.

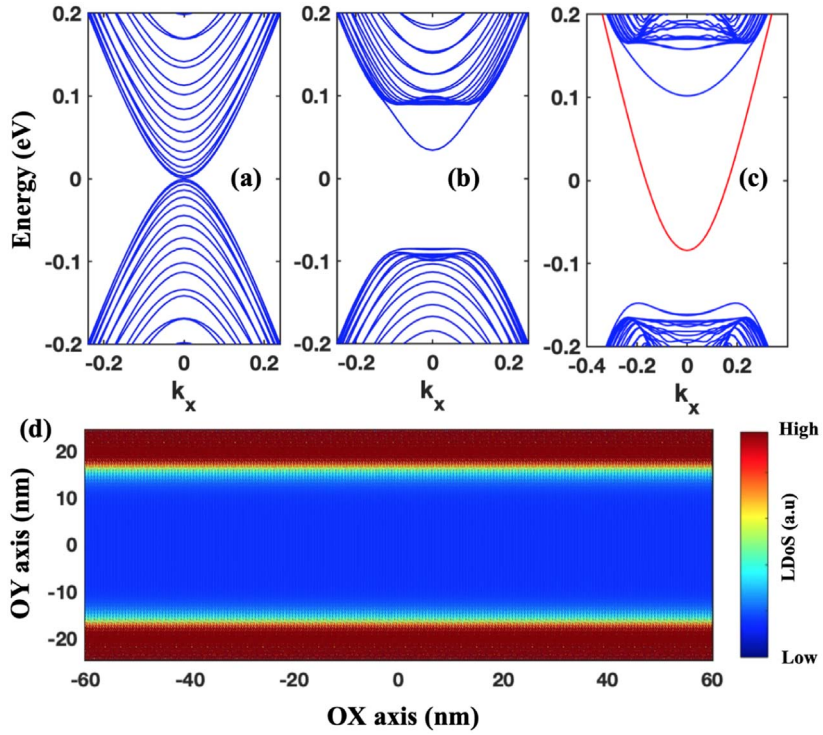

Figure 2. The variation of electronic band structures (a, b, c) and LDoS (d) of a SS-AGNR system where the width of the bottom layer is about 50 nm ($M_b = 200$) and that of the top layer is about 43 nm ($M_t = 174$). Potential $U = 0$ in (a), $U = 0.2$ V in (b) and $U = 0.6$ V in (c, d). LDoS in (d) is calculated for the electronic states of the subband indicated by red in (c) at the Fermi energy of 50 meV.

3.2. Quantum interference

Next we investigate transport properties through our proposed electronic interferometers consisting of hetero-junctions created by applying perpendicular electric fields locally and oppositely to three regions of a SS-AGNR. This structure is similar to the well known FP interferometer for light waves because the junctions will cause electrons to bounce back and forth in the region between two junctions. However, the structure also has features of quantum Hall AB interferometers in that electrons travel in the edges of the sample with inter-edge scattering made possible through 1D electronic channels at the junctions. By varying the Fermi energy of the system, the de Broglie wavelength of electrons will be changed. First, we plot the conductance as a function of the Fermi energy in figure 3(a) which clearly shows the oscillation with peaks and valleys at given Fermi energies. The positions of peaks and valleys are, however, not regularly-spaced because the energy dispersion is not linear as seen in figure 2(c)(red curve). We note also that the Fermi energy is limited to ± 0.1 eV because only electronic states of the subband indicated by red color are considered.

The values of conductance valleys can be as low as zero while those of conductance peaks can be close to 2 (in the unit of $2e^2/h$, because of the two-fold degeneracy of the first subband.) To confirm this, we plot the local density of left-injected electronic states on figure 3(b) at two Fermi energies corresponding to a valley and a peak (marked by the black and red circles, respectively) of the conductance. As can be seen, LDoS in the right region is practically zero for the Fermi energy corresponding to the former, signifying that electrons cannot propagate through the system, while it is as high as two other regions for the latter. The pictures also show that electrons encircle along the edge of device centre (the cavity), similar to that observed in quantum Hall AB interferometers. However, while electrons can only circulate either clockwise or anticlockwise, depending on the direction of the applied magnetic field, in quantum Hall AB interferometers, they can travel in both directions in the structure under study here. Moreover, the LDoS in the central region consists of 'packets' similar to the case of standing waves. All of the features observed in figure 3 are strong indications of quantum interference of electrons when they travel through the structure.

To understand the nature of electron interference, we vary the width of the central region, which plays similar role of FP resonant cavity, and compute the conductance at the peak and valley energies as indicated in figure 3(a). The plots of conductance as a function of N_c are displayed in figure 4. Interestingly, one can see clear and smooth oscillations of conductance when the width of the central region is varied. This can be understood as an analogy of the well-known result for optical FP interferometers [17]. Namely, for an incident light of wavelength, λ, if the width of the cavity is equal to (i) $k\frac{\lambda}{2}$ (standing wave with two nodes at the cavity walls) or (ii)

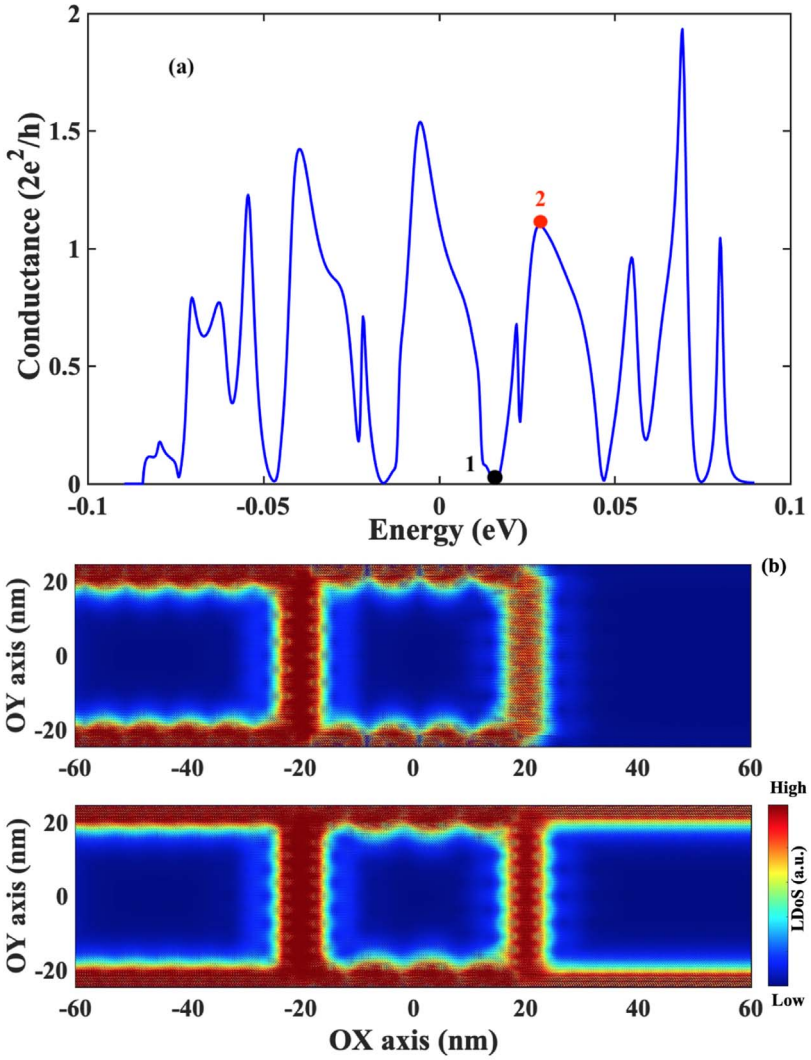

Figure 3. Conductance as a function of the Fermi energy (a) and the local density of left-injected electronic states (b) at two Fermi energies corresponding to a valley and a peak of the conductance as indicated in (a). The hetero-junctions are created by applying electric fields locally and oppositely to a SS-AGNR. Parameters of the structure: $U = 0.6$ V, $M_b = 200$ (~50 nm), $M_t = 174$ (~43 nm), and $N_c = 94$ (~40 nm).

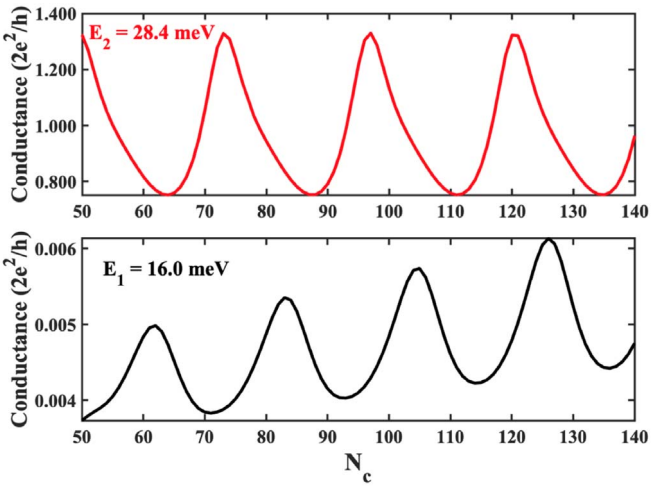

Figure 4. Top panel: conductance as a function of the width of the central region N_c at the energy corresponding to the conductance peak in figure 3(a). Bottom panel: same as the top, but for the case of conductance valley.

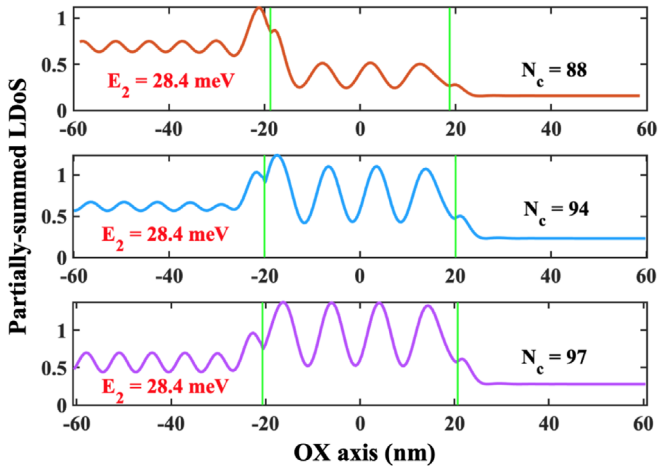

Figure 5. LDoS summed along y-direction as a function of position along the x-direction for 3 different values of N_c. The Fermi energy is fixed at 28.4 meV which corresponds to a conductance peak in figure 3(a). As a guide to the eye, vertical lines near ± 20 nm are draw to indicate positions of the junctions (slightly shifted from top to bottom panels as the width of the middle region increases.)

$k\frac{\lambda}{2} + \frac{\lambda}{4}$ (standing wave with a node and an antinode at the cavity walls; k is a non-negative integer), constructive or destructive interference, respectively, will occur, leading to the oscillation of transmission coefficient. Here, the Fermi energy, i.e. the de Broglie wavelength of electrons, is fixed and the width of the central region is varied, thus conductance maxima and minima were observed when they satisfy the conditions (i) and (ii) for constructive and destructive interference, respectively.

To further support this explanation, we perform a more detailed analysis by summing LDoS along the y-direction in the region near the bottom edge and plot the result along the x-direction. Figure 5 displays the results so-obtained, which is called partially-summed LDoS, for three cases with different values of N_c at the fixed Fermi energy $E_F = 28.4$ meV. At $N_c = 88$ (top panel), the partially-summed LDoS picture shows that a maximum (antinode) and a minimum (node) of LDoS occur almost exactly at the junctions (not perfect because of the contributions from LDoS of the 1D conducting channel along the junctions.) Thus, the condition (ii) is satisfied, i.e. destructive interference occurs which leads to a minimum of the conductance as already seen in the top panel of figure 4. On the contrary, at $N_c = 97$ (bottom panel), the condition (i) is fulfilled, resulting in a maximum of the conductance. At N_c=94 (middle panel), neither (i) nor (ii) is exactly met, so the conductance has an intermediate value.

There is, however, a difference between the interference of electrons in SS-AGNR studied here and that of light in the optical FP interferometer. While transmission coefficient of the latter is 100% whenever the condition (i) is satisfied [17], the conductance of electron tends to oscillate within a range of values, which depends on the energy. To clarify this point, we note that figure 3(b) also shows two regions with high values of LDoS along the $y-$ direction around two junctions. This means that not only can electrons be bounced off the junctions, in much the same way as the light wave does at the partially reflected mirrors in an optical FP interferometer, when they are incident to the junctions but they can also be scattered, via the 1D conducting channel at the junctions, from one edge to the other and vice versa. Thus there will be a possibility that electrons traversing clockwise and anti-clockwise along the boundary of the central region interfere destructively. In this case, the total conductance will be small, regardless of the width of the cavity, as can been seen in the bottom panel of figure 4. To further support this picture, we investigated transport properties through a system with single junction only, i.e. the system consisting of only two regions with opposite electric fields. LDoS along the junction was calculated for different Fermi energies and displayed in figure 6 together with the conductance of the same system. As can be seen clearly in the top panel, LDoS around the junction is enhanced at several values of the Fermi energy, namely $E_F \approx -75, -60, -22, 16, 43, 75$ meV, which correspond to the decreases in the conductance shown in the bottom panel (note that LDoS here is along the junction which is perpendicular to the transport direction.) Moreover, if the electric fields on two sides of the junction are reversed, the obtained pictures of LDoS and conductance will be, as a consequence of band inversion mentioned before, the mirror reflections through the vertical line at the energy $E = 0$. As a result, for the system with two junctions, LDoS will be enhanced around one junction at 8 values of the Fermi energy $E_F \approx \pm 60, \pm 43, \pm 22, \pm 16$ meV and around both junctions at $E_F \approx \pm 75$ meV. Interestingly, the conductance valleys in figure 3(a) occur at these 10 values of the Fermi energy.

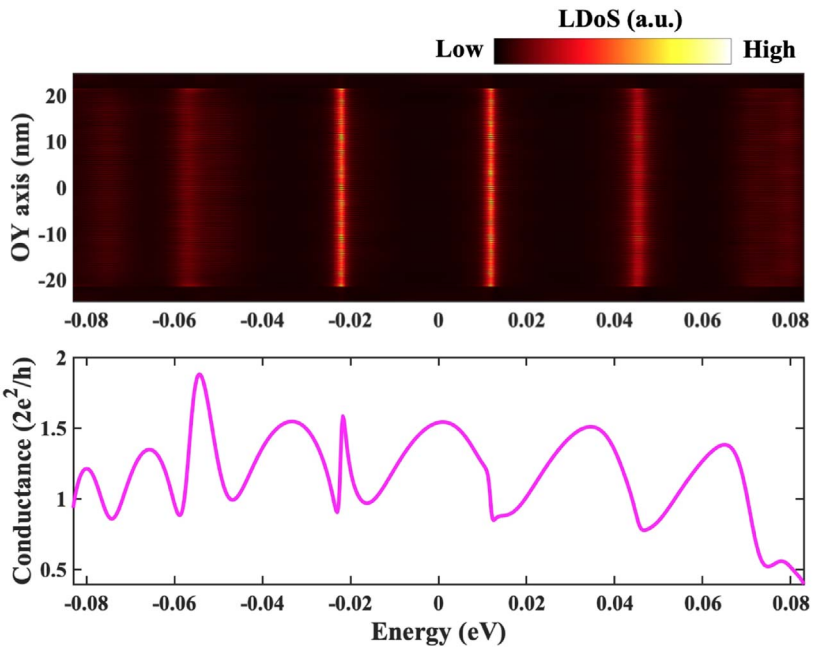

Figure 6. Top panel: LDoS along the junction in the system consisting of two regions with opposite electric fields plotted at different values of the Fermi energy. Bottom panel: Conductance through the single-junction system as a function of the Fermi energy. Calculation parameters: $U = 0.6$ V, $M_b = 200$ (∼50 nm), $M_t = 174$ (∼43 nm).

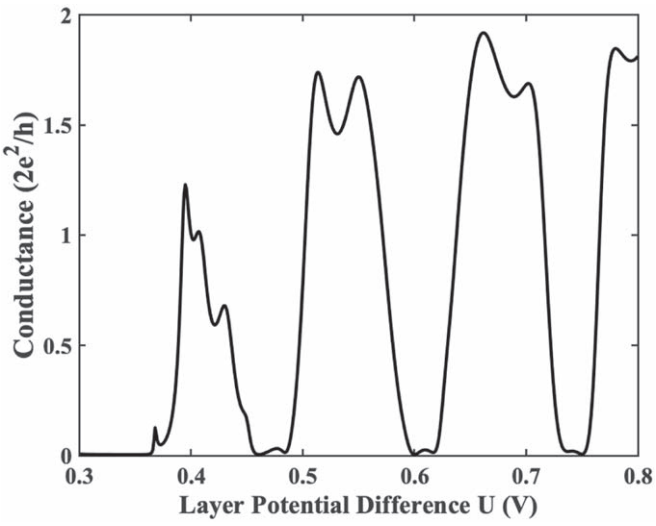

Figure 7. Conductance as a function of electric potential difference between two layers. Calculation parameters: $E_F = 16$ meV, $M_b = 200$ (∼50 nm), $M_t = 174$ (∼43 nm) and $N_c = 94$.

Finally, we investigate the possibility to control the electron transport by tuning the applied electric field strength. In experiment, this can be done efficiently varying the gate voltages. Figure 7 shows the conductance as a function of electric potential difference, U, between two graphene layers computed at the Fermi energy $E_F = 16$ meV. The obtained result shows the variation of conductance over a wide range of values, from minimum values close to zero to maximum ones of nearly 2. It is worth to note that the zero conductance observed in the region with small values of U (less than ~ 3.5 V) is simply because the energy $E_F = 16$ meV stays right in the gap region (see figure 2(b)), while the quantum interference of electrons is responsible for the vanishing conductance at some larger values of U.

4. Conclusions

In this work, a new graphene-based FP interferometer is proposed. Unlike FP quantum Hall interferometers in which electronic edge states are created with the use of strong magnetic fields, the one proposed in this work utilizes the stacked graphene structures consisting of two unequal width, arm-chaired nanoribbons that can induce electronic states residing near two edges when an electric field is applied perpendicularly to the structures. Electronic junctions formed at the interfaces of two oppositely biased regions cause reflection and inter-edge scattering of electrons. The large mean-free path of electrons in graphene can lead to large coherent length which is the necessary condition for electron interference. The proposed FP interferometer is anticipated to be realised in experiment utilizing the widely-used local gate techniques in fabricating graphene-based devices.

Our numerical simulations based on a tight-binding model within the Landauer's formalism show the oscillations in electron conductance, indicating the quantum interference of electron in the system. While electrons bouncing back and forth between two junctions cause the interference similar to that of light waves in optical FP interferometers, the inter-edge scattering affects this interference picture significantly. Specifically, at energies where 1D conducting channels at the junctions allows for strong inter-edge scattering, electron transmission between two edges causes destructive interference, resulting in very small values of the total conductance. We expect that the large variation of conductance when changing the applied electric field would allow for the possibility to observe and control electron interference in the proposed FP interferometer in experiment.

Acknowledgments

We thank V. Hung Nguyen for useful discussions and helpful comments on the manuscript. This research is funded by Graduate University of Science and Technology (GUST), Vietnam Academy of Science and Technology, under grant number GUST.STS.DT.2020-VL01.

Data availability statement

The data that support the findings of this study are available upon reasonable request from the authors.

ORCID iDs

Huy-Viet Nguyen https://orcid.org/0000-0002-5509-0061

References

[1] Aharonov Y and Bohm D 1959 *Phys. Rev.* **115** 485
[2] Tonomura A, Osakabe N, Matsuda T, Kawasaki T, Endo J, Yano S and Yamada H 1986 *Phys. Rev. Lett.* **56** 792
[3] Von Klitzing K 1986 *Rev. Mod. Phys.* **58** 519
[4] Novoselov K S, Geim A K, Morozov S V, Jiang D e, Zhang Y, Dubonos S V, Grigorieva I V and Firsov A A 2004 *Science* **306** 666–9
[5] Neto A C, Guinea F, Peres N M, Novoselov K S and Geim A K 2009 *Rev. Mod. Phys.* **81** 109
[6] Young A F and Kim P 2009 *Nat. Phys.* **5** 222–6
[7] Gusynin V and Sharapov S 2005 *Phys. Rev. Lett.* **95** 146801
[8] Zhang Y, Tan Y W, Stormer H L and Kim P 2005 *Nature* **438** 201–4
[9] Morikawa S, Masubuchi S, Moriya R, Watanabe K, Taniguchi T and Machida T 2015 *Appl. Phys. Lett.* **106** 183101
[10] Mreńca-Kolasińska A, Heun S and Szafran B 2016 *Phys. Rev.* B **93** 125411
[11] Wei D S, van der Sar T, Sanchez-Yamagishi J D, Watanabe K, Taniguchi T, Jarillo-Herrero P, Halperin B I and Yacoby A 2017 *Science Adv.* **3** e1700600
[12] Makk P *et al* 2018 *Phys. Rev.* B **98** 035413
[13] Nguyen V H and Charlier J C 2019 *2D Mater.* **6** 045045
[14] Nguyen V H and Charlier J C 2020 *Nanoscale Adv.* **2** 256–63
[15] Özyilmaz B, Jarillo-Herrero P, Efetov D, Abanin D A, Levitov L S and Kim P 2007 *Phys. Rev. Lett.* **99** 166804
[16] Banszerus L, Schmitz M, Engels S, Goldsche M, Watanabe K, Taniguchi T, Beschoten B and Stampfer C 2016 *Nano Lett.* **16** 1387–91
[17] Vaughan J M 2017 *The Fabry-Perot Interferometer: History, Theory, Practice and Applications* (Routledge)
[18] Rickhaus P, Maurand R, Liu M H, Weiss M, Richter K and Schönenberger C 2013 *Nat. Commun.* **4** 1–6
[19] Varlet A *et al* 2014 *Phys. Rev. Lett.* **113** 116601
[20] Jiang Y, Mao J, Moldovan D, Masir M R, Li G, Watanabe K, Taniguchi T, Peeters F M and Andrei E Y 2017 *Nat. Nanotechnol.* **12** 1045–9
[21] Brun B, Nguyen V H, Moreau N, Somanchi S, Watanabe K, Taniguchi T, Charlier J C, Stampfer C and Hackens B 2021 *Nano Lett.* **22** 128–34
[22] Shytov A V, Rudner M S and Levitov L S 2008 *Phys. Rev. Lett.* **101** 156804
[23] Zhang Y, Tang T T, Girit C, Hao Z, Martin M C, Zettl A, Crommie M F, Shen Y R and Wang F 2009 *Nature* **459** 820–3

[24] Martin I, Blanter Y M and Morpurgo A 2008 *Phys. Rev. Lett.* **100** 036804
[25] Vaezi A, Liang Y, Ngai D H, Yang L and Kim E A 2013 *Phys. Rev.* X **3** 021018
[26] McCann E and Koshino M 2013 *Rep. Prog. Phys.* **76** 056503
[27] Lewenkopf C H and Mucciolo E R 2013 *J. Comput. Electron.* **12** 203–31
[28] Hung Nguyen V, Saint-Martin J, Querlioz D, Mazzamuto F, Bournel A, Niquet Y M and Dollfus P 2013 *J. Comput. Electron.* **12** 85–93
[29] Sancho M L, Sancho J L and Rubio J 1984 *J. Phys. F: Metal Phys.* **14** 1205
[30] Taychatanapat T and Jarillo-Herrero P 2010 *Phys. Rev. Lett.* **105** 166601